Ultrafast Thermal Switching Enabled by Transient Polaritons

Bei Yang, Bai Song, F. Javier García de Abajo,* and Qing Dai*

ABSTRACT: **Ultrafast thermal switches are pivotal for managing heat generated in advanced solid-state applications, including high-speed chiplets, thermo-optical modulators, and on-chip lasers. However, conventional phonon-based switches cannot meet the demand for picosecond-level response times, and existing near-field radiative thermal switches face challenges in efficiently modulating heat transfer across vacuum gaps. To overcome these limitations, we propose an ultrafast thermal switch design based on pump-driven transient polaritons in asymmetric terminals. Demonstrated with WSe_2 and graphene, this approach achieves an impressive thermal switching ratio exceeding 10,000 with response times on the picosecond scale, outperforming current designs by at least 2 orders of magnitude. This exceptional performance is driven by dynamic polaritonic coupling between terminals, activated by ultrafast photoexcitation. Additionally, the WSe_2 monolayer-based switch exhibits a laser cooling effect, enabled by enhanced carrier excitation efficiency and prolonged carrier lifetimes, introducing a disruptive mechanism for laser cooling. Our findings highlight the strong potential of photodriven transient polaritons in advancing ultrafast thermal switches and nanoscale cooling technologies.**

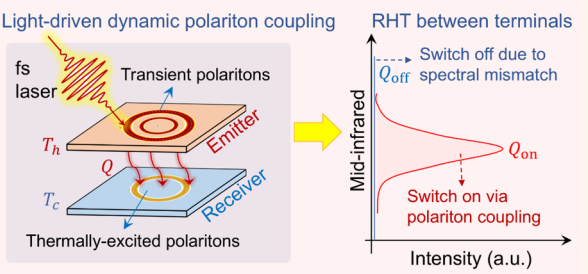

KEYWORDS: *ultrafast thermal switch, transient polaritons, two-dimensional materials, near-field radiative heat transfer, laser cooling*

INTRODUCTION

As transistor sizes shrink below 10 nm, the ever-growing miniaturization and complexity of electronic devices places thermal management at the forefront of challenges in microelectronics. Ultrafast thermal switches, capable of rapidly regulating heat flow in response to external stimuli, are increasingly critical for applications such as high-speed chiplets, thermo-optical modulators, on-chip lasers, thermal logic circuits, and magnetic refrigeration.[1−5] Their integration into high-speed photoelectronic chips,[6,7] for example, can mitigate heat buildup, reduce thermal crosstalk, and prevent thermal damage. Achieving such functionality requires synchronously implementing rapid internal heat transfer and high-speed modulation of external control fields.

Extensive research has focused on improving the response times of thermal switches. Solid-state approaches, which modulate material thermal conductivities using external fields, primarily rely on phonons for heat transfer and exhibit response times ranging from seconds to minutes[4,8−20] (see supplementary Table S1). For instance, thermal-field-regulated designs typically respond on the scale of seconds.[10,15] Recent innovations, such as a self-assembled molecular switches with high-speed electronic gating, have pushed response times to microsecond ranges.[18] Advances in antiferroelectric[19] and superconducting[4] thermal switches have further achieved response times of 150 and 15 ns, respectively, through faster voltage pulses and optimized phonon transport.

Thermal radiation offers a promising alternative for ultrafast thermal switching, benefiting from the inherent speed of photon-based heat transfer compared to phonon- or electron-mediated mechanisms.[21−25] Near-field radiative thermal switches, driven by electric or optical fields, can leverage coupled optical modes between terminals to achieve faster responses.[26] However, current symmetric designs[22−24] face challenges in effectively decoupling heat transfer channels, limiting their ability to switch off radiative modes efficiently.

Here, we propose an ultrafast thermal switch design based on transient polaritons—short-lived hybrid light-matter quasiparticles generated by femtosecond laser pulses.[27−29] By employing an asymmetric terminal configuration, this design provides versatility, enabling the integration of diverse materials. Exemplified by integrating WSe_2 with graphene across a vacuum gap, we exploit the mismatch in their radiative

spectra to suppress heat transfer in static conditions (without laser pumping). Through precise pump-driven manipulation of transient exciton polaritons within WSe_2, we facilitate efficient switching of near-field radiative heat transfer (RHT) channels. This approach demonstrates exceptional performance, achieving a thermal switching ratio exceeding 10,000 with picosecond-level response times. The key to this dynamic switching lies in the time-varying polaritonic coupling between the terminals, initiated by external ultrafast photoexcitation. Notably, the WSe_2 monolayer -based switch also enables a laser cooling effect, leveraging enhanced exciton excitation efficiency and prolonged carrier lifetimes, introducing a disruptive mechanism for laser cooling. This work highlights the significant potential of photodriven transient polaritons for ultrafast thermal modulation as well as nanoscale cooling technologies.

RESULTS AND DISCUSSION

Generalized Design Concept for Ultrafast Thermal Switching. Figure 1a illustrates the generalized design concept for ultrafast thermal switching based on transient polaritons. While traditional methods like electrical gating or chemical doping can manipulate the dielectric responses of materials in the mid-infrared (MIR) range, they are typically too slow for advanced applications requiring faster response times. Therefore, we utilize ultrafast optical pumping to achieve rapid control of heat transfer. The system under investigation is a biplanar radiative thermal switch with asymmetric terminals separated by a vacuum gap. An optical pump pulse is directed at the emitter terminal, exciting a high density of carriers within the material. This carrier excitation alters the dielectric response of the emitter, which evolves dynamically over time. As the dielectric response changes, it influences the polaritonic coupling between the terminals, leading to significant variations in both the spectral and amplitude distributions of the RHT flux.

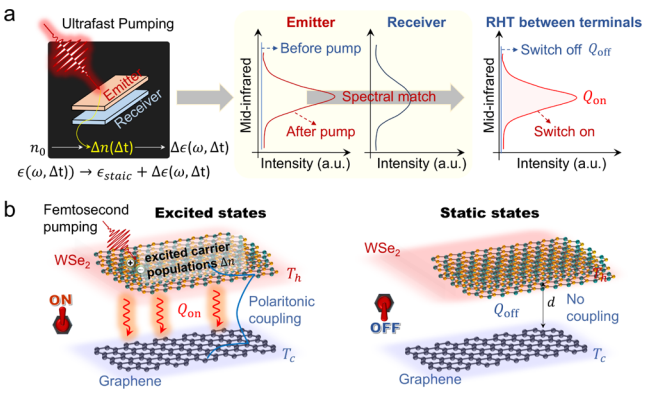

Figure 1. Schematic of ultrafast thermal switching via pump-induced transient polaritons. (a) Design principle: the mechanism involves asymmetric terminals, where photoexcited carriers (Δn) in the emitter induce a transient MIR response that spectrally aligns with the receiver. This alignment leads to strong polaritonic coupling, thereby activating previously unavailable RHT channels. (b) Feasible configuration for practical demonstration: we consider WSe_2 as the emitter and graphene as the receiver, separated by a vacuum gap (d). In the "on" state (left panel), optical pumping of the emitter generates polaritonic coupling (Q_{on}), which contrasts with the "off" state (right panel) where no coupling occurs (Q_{off}). This significant difference in RHT flux between these two states, triggered by laser-pulse irradiation, demonstrates the ultrafast thermal switching process.

We apply this concept to a model system where WSe_2 and graphene are used as asymmetric terminals across a vacuum gap (Figure 1b). In this configuration, WSe_2 is maintained at a higher temperature, T_h, acting as the emitter; while graphene is kept at a lower temperature, T_c, serving as the receiver. The temperature difference, $\Delta T = T_h - T_c$, drives a net flow of heat between the terminals. Upon exposure to femtosecond laser pulses, WSe_2 undergoes the excitation of a high density of electron−hole pairs, which in turn modifies the material's dielectric response and triggers the creation of transient exciton polaritons.

These polaritons then couple with surface plasmon polaritons in graphene, significantly enhancing the near-field RHT flux across the gap, denoted as Q_{on}. This coupling activates the thermal switch, transitioning it into the "on" state and facilitating efficient heat flow between the terminals, as shown in the left panel of Figure 1b. When the optical pumping ceases and the photoexcited hot carriers fully decay, the system returns to its static configuration. In this state, the polaritonic coupling (and ensuing RHT) is severed due to the spectral mismatch between the two terminals, resulting in a reduced heat flux, Q_{off}. This corresponds to the "off" state of the thermal switch, depicted in the right panel of Figure 1b.

Thus, this design enables ultrafast thermal switching through optical pumping, which drives the RHT transition between the "on" and "off" states. Note that in our theoretical model, the dimensions of both terminals are tailored to match the laser spot size, optimizing light-matter interaction and ensuring efficient thermal switching.

To quantify the performance of the thermal switch, define the thermal switching ratio (TSR), denoted as r, as follows:[3,8]

$$r = \frac{Q_{on}}{Q_{off}} \tag{1}$$

where Q_{on} is the RHT flux for the "on" state, while Q_{off} is the flux in the "off" state. The TSR measures the heat flux contrast between the on and off states, providing a clear indication of the switch's effectiveness. Furthermore, we evaluate the responsiveness of the switch to external stimuli by analyzing the time period, τ, during which the switch can transition between the on and off states. This response time assesses the switch's ability to rapidly adapt to dynamic environments, a key factor for its practical application in ultrafast thermal management.

Modulating the Dielectric Response of WSe_2 through Ultrafast Photoexcitation. WSe_2 is a transition metal dichalcogenide (TMD),[30−32] a class of materials characterized by a layered structure, where strong covalent bonds exist within each layer, while weak van der Waals (vdW) forces hold the layers together. The strong anisotropy inherent in this structure translates into its optical properties, which can be described by a diagonal anisotropic dielectric tensor, given by[33]

$$\|\varepsilon\| = \begin{bmatrix} \epsilon^x & 0 & 0 \\ 0 & \epsilon^y & 0 \\ 0 & 0 & \epsilon^z \end{bmatrix} \tag{2}$$

Where, $\epsilon^x = \epsilon^y$ represents the in-plane components, while ϵ^z denotes the out-of-plane component.

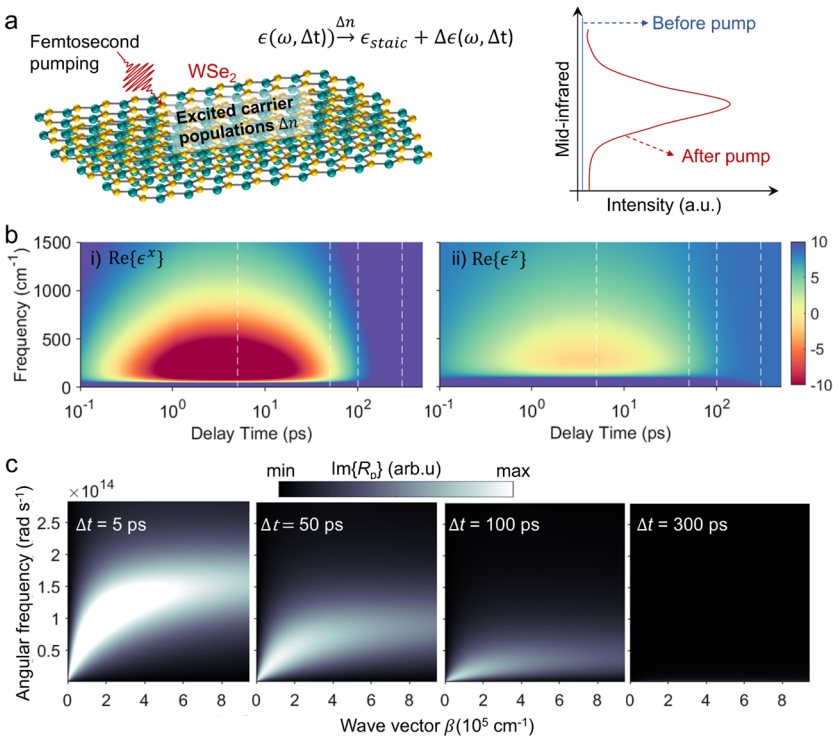

Figure 2. Transient dielectric response of WSe_2 following femtosecond optical pumping. (a) Schematic of the fundamental processes considered in the model. (b) Real parts of the (i) in-plane and (ii) out-of-plane dielectric tensor components of WSe_2, plotted against frequency and delay time for a photoexcited carrier density of 3.2×10^{19} cm^{-3} at 400 K. White vertical dashed lines indicate delay times of 5, 50, 100, and 300 ps. (c) Corresponding evolution of polaritonic dispersions in a 5 nm-thick WSe_2 film at various delay times.

The dielectric tensor ϵ^i describes how WSe_2 interacts with light at different frequencies and temperatures. Importantly, this tensor can be influenced by external stimuli such as an ultrafast laser pulse, resulting in a transient response that can be written as

$$\epsilon^i(\omega, T, \Delta t) = \epsilon^i_{stat}(\omega, T) + \Delta\epsilon^i(\omega, T, \Delta t) \quad (3)$$

Here, ω denotes the photon energy, T is the temperature before pumping, and Δt is the delay time relative to the applied pulse. This equation separates the static response (ϵ^i_{stat}) from the transient modifications ($\Delta\epsilon^i$) induced by photoexcited states within the material. The superscript i indicates components of the dielectric tensor along specific directions (i.e., x, y, or z). Each transient modification $\Delta\epsilon^i$ is approximately linear with the photoexcited exciton density $n_i(\Delta t)$ and can be expressed using a classical Drude-Lorentz as[34−37]

$$\Delta\epsilon^i(\omega, \Delta t) = \frac{n_i(\Delta t)e^2}{m^i\epsilon_0} \sum_j \frac{f^i_j}{\omega_j^2 - \omega(\omega + i\gamma_j)} \quad (4)$$

In this model, e is the elementary charge, m^i the effective carrier mass for propagation along the direction i, and ϵ_0 is the vacuum permittivity. The summation incorporates various transitions within the material, indexed by j, each treated as a damped oscillator with oscillator strength f^i_j, resonance frequency ω_j, and damping rate γ_j. The specific resonant frequencies and strengths of these transitions are taken from in ref.[38] Our results rely on this spectral profile, assuming the order of magnitude is correct for the model.

To quantify the exciton density generated by the optical pump, we assume that each absorbed pump photon excites one exciton. The volume density of photoexcited excitons n_x can be determined as

$$n_x = \frac{\alpha F_0}{\hbar\omega_0 t_{WSe2}} \quad (5)$$

where α is the absorbance, F_0 is the pump fluence, ω_0 is the pump photon energy, and t_{WSe2} is the thickness of the WSe_2 layer. By adjusting F_0, we can control n_x, and thereby modulate the dielectric properties of WSe_2. For the specific systems investigated here, which consist of WSe_2 and graphene separated by a gap, the pump-induced energy absorption per pulse and exciton excitation are analytically quantified, as described in S3 of the Supporting Information (SI).

While the intricate processes of photon absorption and exciton generation are beyond the scope of this discussion, our calculations assume a pump photon energy slightly below the bandgap of WSe_2. This approach ensures that the thermal energy associated with exciton formation is equivalent to the absorbed light energy. Furthermore, we model the exciton density decay over time as an exponential process, expressed as $n_i(\Delta t) = n_i(0)\exp\left\{\frac{-\Delta t}{\tau_e}\right\}$, where τ_e is the characteristic exciton decay time. This model allows us to compare the cumulative RHT energy per cycle with the energy absorbed from each pump pulse, facilitating a comprehensive analysis of the energy dynamics in the device.

Transient Hyperbolicity in WSe_2 Following Ultrafast Photoexcitation. We begin by examing the light absorption efficiency of the material terminals, i.e., WSe_2 and graphene, under a pump laser with a photon energy of 1.59 eV (Figure 2a). The absorption in graphene is significantly lower than that in WSe_2, and this disparity becomes more pronounced as the

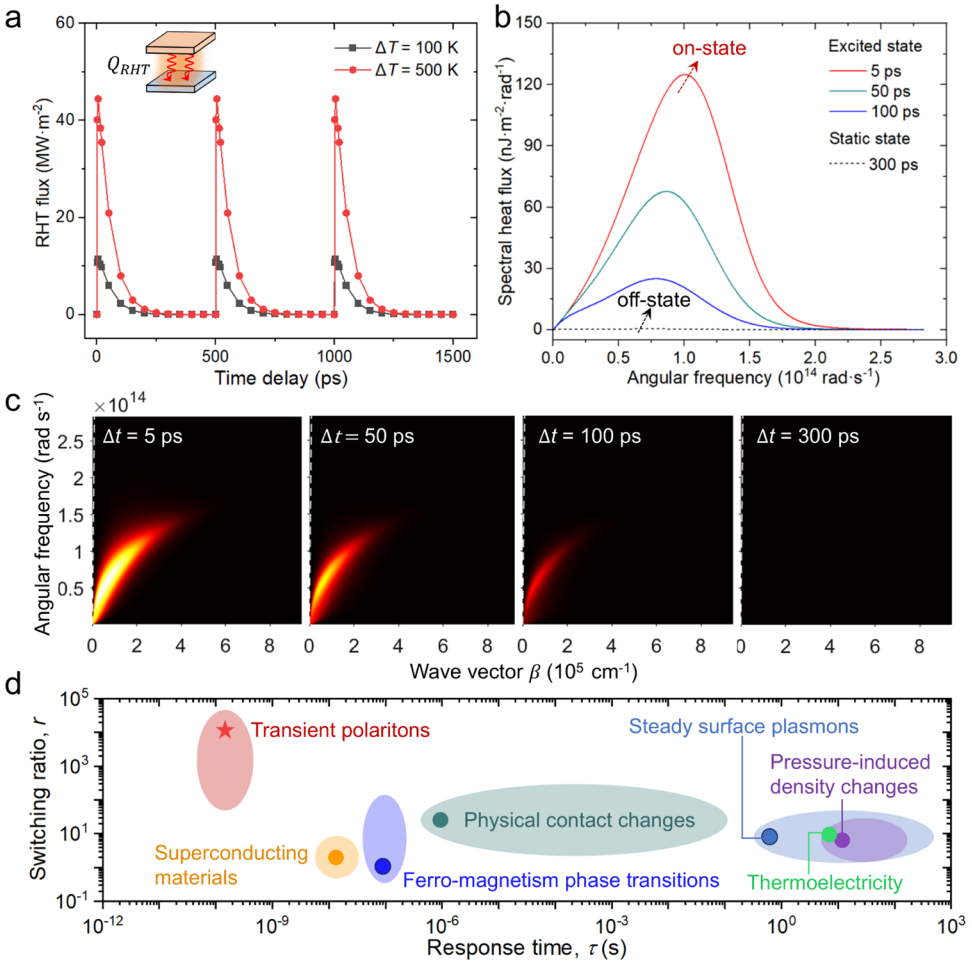

Figure 3. Ultrafast thermal switching in the WSe_2–graphene system. (a) ***Ad hoc*** **superposition of three replicas of the calculated transient RHT flux for temperature differences ΔT = 100 and 500 K, illustrating that the effect of each cycle has decayed fully before the next begins at a laser repetition rate of 2 GHz.** (b) **Spectral decomposition of the RHT flux at various time delays.** (c) **Corresponding PTP contour maps as a function of frequency and wave vector, with white dashed lines indicating the vacuum light line.** (d) **Chart comparing the thermal switching ration r versus response time τ in our design based on transient polaritons and in existing designs utilizing mechanisms such as ferro-magnetism phase transitions,[12−14,19] physical contact changes,[15−18] superconducting materials,[4] thermoelectricity,[10] mass density changes,[8,9] and steady surface plasmons.[22−25] Detailed data are provided in Table S1.**

thickness of WSe_2 increases (Figure S2), rendering its effects on the switch's performance negligible. In contrast, WSe_2 exhibits increasing light absorption with thickness, peaking at approximately 25 nm (Figure S3). However, thicker WSe_2 layers reduce the volumetric exciton density (n_x), suggesting that a monolayer of WSe_2 is most efficient for generating excitons per unit volume. Figure S4 shows the relationship between the pump fluence (F_0) and n_x for both a WSe_2 monolayer and a 5 nm-thick layer. We also consider the Mott transition, where high exciton densities can lead to a metallic state rather than distinct excitons. For WSe_2 monolayers, this transition occurs at exciton densities around $10^{20} - 10^{21}$ cm^{-3}.[39] The fluence values used in this study are sufficiently low to keep n_x below this threshold, avoiding the Mott transition.[36] Figure S5 shows the temporal evolution of exciton density in both monolayer and 5 nm WSe_2 following a 500 fs laser pulse. These results provide the basis for analyzing the transient dielectric tensor of WSe_2, which underpins the thermal switching mechanism.

Figure 2b presents the real components of the in-plane ($\mathrm{Re}\{\epsilon^x\}$ = Re $\{\epsilon^y\}$) and out-of-plane ($\mathrm{Re}\{\epsilon^z\}$) dielectric tensor for 5 nm WSe_2 as a function of time delay (Δt) and optical frequency (ω) after laser excitation. It has been well established that photoexcited electron–hole pairs in WSe_2 form discrete excitonic states, which then couple to photons to create exciton polaritons through quantum transitions.[37,38] Since the energies of these excitonic transitions typically fall in the range of tens of meV, the resulting transient polaritonic responses occur in the MIR range.[40] The in-plane response (Figure 2b-i) exhibits a pronounced dip in $\mathrm{Re}\{\epsilon^x(\omega)\}$ across a broad mid-IR range, reaching negative values immediately after excitation. This negative permittivity diminishes as carrier density decays, with the affected frequency range narrowing over time. In contrast, the out-of-plane response (Figure 2b-ii) remains consistently positive in the same frequency range. The contrasting signs of $\mathrm{Re}\{\epsilon^x(\omega)\}$ and $\mathrm{Re}\{\epsilon^z(\omega)\}$, i.e., $\mathrm{Re}\{\epsilon^x(\omega)\}$ $\mathrm{Re}\{\epsilon^z(\omega)\} < 0$, highlight hyperbolic dispersion, driven by ultrafast optical pumping and the inherently anisotropic optical properties of WSe_2.

To further explore the transient hyperbolic dispersion in WSe_2, we analyze the momentum-dependent reflection coefficient, $\mathrm{Im}\{R_p\}$, calculated using the dielectric tensor from Figure 2b. By tracking the maxima of $\mathrm{Im}\{R_p\}$ across various frequencies and wave vectors, we map the polaritonic

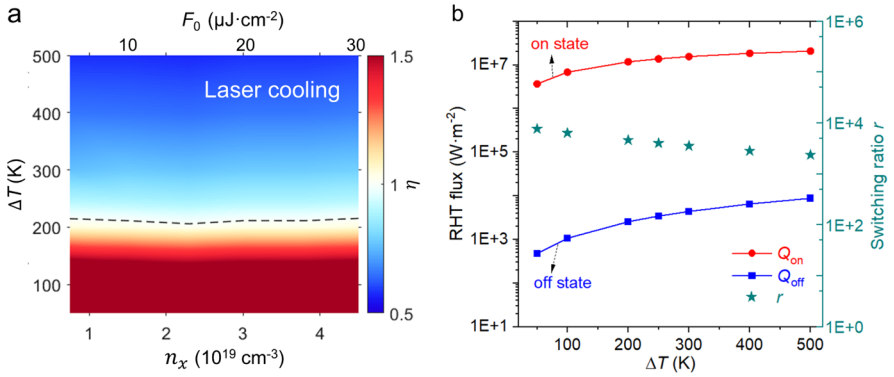

Figure 4. Laser cooling effect and tunable performance of the ultrafast thermal switch. (a) Ratio of absorbed energy density to RHT flux, $\eta = Q_{abs}/\Delta Q_{RHT}$, plotted against carrier density (n_x) and static temperature difference (ΔT). The dashed black line represents $\eta = 1$, with $\eta < 1$ (blue region) indicating laser cooling. (b) Distributions of on- and off-state RHT flux, along with the corresponding switching ratio (r) as a function of ΔT. Calculations are performed for the following parameters: $T_c = 300$ K, $d = 10$ nm, $\mu = 0.05$ eV, $t_{WSe2} = 0.7$ nm,and $n_x = 3.8 \times 10^{19}$ cm^{-3}.

dispersion relation in WSe_2. Figure 2c visualizes these polaritons as bright bands in momentum-energy ($k_{\parallel} - \omega$) space. The bands redshift to lower frequencies and narrow in bandwidth as the delay time increases from 5 to 100 ps, ultimately vanishing by 300 ps. The hyperbolic nature of WSe_2 allows these polaritons to exist at large wave vectors, underscoring the material's unique optical properties.

Ultrafast Thermal Switching and Underlying Mechanisms. Our investigation leverages photoexcited transient exciton polaritons in WSe_2 to achieve ultrafast thermal switching. A pivotal task in this endeavor is to identify a material that spectrally aligns with the transient hyperbolic polaritons in photoexcited WSe_2. Graphene emerges as an ideal candidate due to its exceptional properties, including atomic-layer thickness, broad infrared response, strong field localization, and tunable plasmonic modes.[41,42] These attributes make graphene particularly effective for modulating near-field RHT, thereby facilitating efficient thermal switching.[26]

Figure 3a showcases the thermal switching effect in a system combining a 5 nm WSe_2 film and a monolayer graphene, separated by a 10 nm vacuum gap. The hot and cold terminals are maintained at fixed temperatures of 400 and 300 K, respectively. For clarity, three on-and-off cycles are replicated in Figure 3a for visualization purposes, emphasizing the switch's capability for dynamic thermal control. In practice, this behavior can be readily achieved with a laser pulse repetition rate of 2 GHz, ensuring that the effects of each cycle (i.e., the RHT rate) dissipates before the next cycle begins.

Intriguingly, the RHT flux profile during a single switching cycle mirrors the dynamics of photoexcited carriers in WSe_2 (Figure S5a), highlighting the central role of carrier behavior in determining performance. At a carrier density of 3.2×10^{19} cm^{-3}, the switch ahieves a peak heat flux of ~11 MW m^{-2} at 5 ps under $\Delta T = 100$ *K*. As the carriers deplete, the system returns to its static state, resulting in a minimal RHT flux of ~1,064 W m^{-2}. This switching mechanism yields an exceptional TSR of ~10,000 over a complete on-and-off cycle of 500 ps, surpassing existing thermal switches by 2 orders of magnitude (Figure 4d). The superior performance in both TSR and response time demonstrates the great potential of our approach.

Note that the performance of our ultrafast thermal switch is influenced by factors such as laser pulse parameters (duration, fluence) and the dynamics of photoexcited carriers in WSe_2. The carrier density dictates the maximum on-state RHT, while the carrier lifetime controls the on-state duration, thereby influencing the response time. Extending the carrier lifetime can enhance the cumulative RHT flux per cycle. For instance, increasing the carrier lifetime in the monolayer to 500 ps[32,43] could significantly improve the on-state flux (Figure S7). However, this improvement comes at the cost of slower response times, potentially limiting the switch's application in ultrafast thermal modulation. This trade-off underscores the importance of balancing carrier density and lifetime to optimize performance. Future research could explore advanced material engineering, hybrid system designs, or other strategies to decouple these parameters, paving the way for enhanced thermal switch performance.

It is crucial to emphasize that our thermal switch excels in the rapid modulation of RHT flux rather than directly controlling temperature. Given the inherent thermal inertia of most systems, immediate temperature adjustments are impractical. Instead, our switch allows for precise engineering of thermal energy distributions before significant temperature changes occur, enhancing its utility in a wide range of applications.

Further insight into the underlying physical mechanisms behind our proposed ultrafast thermal switching is provided by the spectral and wave-vector decomposition of the RHT flux, shown in Figure 3b. The dominant heat transfer region is associated with the MIR range, particularly below 2.0×10^{14} rad·s^{-1}. Following photoexcitation, the RHT flux peaks at 5 ps. Over time, the spectral bandwidth narrows, and the amplitude decreases, leading to a decline in RHT flux, as observed in Figure 3a. This trend continues until the photoexcited carriers are depleted, and the system returns to its off state.

Figure 3c complements these findings by presenting contour maps detailing the spectral and wave-vector decomposition of the RHT flux. After photoexcitation, bright bands appear, with changing intensity and width over time, representing PTP mediated by polaritonic coupling between the terminals. These bands exhibit a redshift and narrowing as the excited states decay, ultimately disappearing as the system returns to its static state. This evolution mimics the transient polaritonic dispersion behavior observed in Figure 2c and confirms that the ultrafast thermal switching is fundamentally linked to the changes in these polaritonic modes induced by the rapid excitation and subsequent decay of carriers in WSe_2. Additional

information provided in Figure S8 of SI further supports the connection between dispersion changes and polaritonic coupling dynamics, underscoring their significance for ultrafast thermal switching.

Laser Cooling and Tunable Performance of the Thermal Switch. We proceed to quantify the cooling rate facilitated by near-field RHT during a single on-and-off cycle of the thermal switch. This involves integrating the time-varying RHT flux, denoted as $Q(t)$, over time within the switching period τ_p, that is, $\Delta Q_{\mathrm{RHT}} = \int_0^{\tau} Q(t)dt$. As depicted in Figure 3a, with a switching period τ of 500 ps and a static temperature difference ΔT of 100 K, ΔQ_{RHT} is calculated to be ~0.8 mJ m^{-2}. This value corresponds to an average heat flux density of about 1.6 MW m^{-2}, which significantly exceeds the conventional far-field limit for a 10 μm gap (approximately 590 W·m^{-2}) by a factor exceeding 2,700. However, ΔQ_{RHT} in this scenario is considerably lower than the absorbed light energy, which is 32.2 mJ m^{-2} (Figure S2). Even if ΔT is elevated to 500 K, the resulting ΔQ_{RHT} of about 2.75 mJ m^{-2} remains substantially lower. This discrepancy can be attributed to the relatively low efficiency of carrier excitation and their short lifetime. Under these conditions, the net effect of optical pumping is to heat the system.

We investigate the possibility of laser cooling in ultrafast thermal switches using monolayer WSe_2. To quantify this effect, we define a parameter η as the ratio of absorbed light density (Q_{abs}) to time-integrated RHT flux (ΔQ_{RHT}): $\eta = \frac{Q_{\mathrm{abs}}}{\Delta Q_{\mathrm{RHT}}}$. Figure 4a presents a color map of this ratio as a function of n_x and ΔT. The black dashed line ($\eta = 1$) indicates the equilibrium region, where $Q_{\mathrm{abs}} = \Delta Q_{\mathrm{RHT}}$. Blue-colored regions, where $\eta < 1$, correspond to conditions under which laser cooling occurs, particularly at elevated temperatures. We attribute this phenomenon to the fact that higher temperatures activate more phonon modes, leading to a larger absolute increase in RHT. However, this effect must be balanced against the accelerated decay of carriers at higher temperatures. Interestingly, the laser cooling effect remains relatively independent of n_x: while higher values of n_x demand higher fluence F_0 (Figure S4), both Q_{abs} and ΔQ_{RHT} increase proportionally, thus maintaining the ratio η. These results suggest that a strategic adjustment of operational parameters could significantly enhance the cooling efficiency, potentially enabling strong laser cooling under suitable conditions.

In the above calculations, we carefully account for the temperature dependence of the transient dielectric tensor in WSe_2. Figure S6 shows the evolution of 2D maps of $\mathrm{Re}\{\epsilon^x(\omega)\}$ in $\omega - \Delta t$ space across various lattice temperatures of the emitter (T_h). We focus on negative regions of $\mathrm{Re}\{\epsilon^x(\omega)\}$, which correspond to the existence (and excitation) of polariton modes. Upon elevating T_h from 400 to 800 K, the intensity of these negative regions decreases, with narrowed frequency and delay time ranges. This trend suggests that the polaritonic response of WSe_2 is highly sensitive to lattice temperature. Higher temperatures lead to stronger phonon interactions, causing faster polariton dephasing and shorter lifetimes. Understanding this temperature dependence is crucial for evaluating polariton behavior, which directly impacts the performance of the thermal switch. For instance, Figure 4b shows a notable decrease in the TSR from about 7,700 to 2,400 (roughly three times lower) when ΔT is raised from 50 to 500 K, despite a slight increase in the on-state RHT flux. These observations underscore the need for a delicate balance between operation temperatures and thermal switch optimization.

Our ultrafast thermal switch offers not only exceptional performance but also remarkable tunability. This tunability can be achieved through both passive (e.g., by varying the WSe_2 thickness) and active (e.g., by adjusting the chemical potential of graphene) approaches (Figure S9). Moreover, the versatility of this design extends beyond the specific materials used in this study. A variety of alternative materials, such as α-MoO_3, hBN, SiO_2, and related heterostructures,[44,45] etc., can potentially replace graphene as the receiver. These materials support surface phonon polaritons in the MIR range, allowing interaction with the transient polaritons photoexcited in WSe_2. Similarly, WSe_2 as the emitter can be substituted by black phosphorus,[27,46] other TMDs,[47] or even entirely different materials[29,48] with comparable optical properties that can be dynamically modulated through optical pumping. This inherent flexibility underscores the broad applicability of our thermal switch platform. By customizing the material selection and operational parameters, the switch can be adapted to meet the specific requirements of various applications, paving the way for advancements in ultrafast thermal management across diverse technological fields.

While the present work is focused on theoretical modeling, an experimental validation is essential to demonstrate the practicality of the proposed thermal switch. Addressing the challenges associated with such experiments requires advanced near-field thermal-measurement setups with picosecond temporal resolution, robust material fabrication techniques to ensure high-quality interfaces, and integration of high-repetition-rate ultrafast laser systems to enable dynamic polaritonic control. Our theoretical findings not only provide a strong foundation for understanding these phenomena but also serve as a roadmap to stimulate and guide future experimental efforts. These efforts will bring this concept closer to realization and amplify its potential impact in ultrafast photonic and thermal technologies.

CONCLUSIONS

This study introduces an ultrafast thermal switch that leverages photodriven transient polaritons in an asymmetric terminal configuration. We demonstrate this concept by pairing WSe_2 with graphene across a vacuum gap, a configuration that achieves a record-high thermal switching ratio of 10^4 within a picosecond time scale. The switch not only delivers impressive performance but also offers significant advantages, including a remarkable near-field radiative cooling rate of ~1.6 MW m^{-2} for a 5 nm-thick WSe_2 terminal, along with the potential for laser cooling in WSe_2 monolayers. These features, combined with noncontact operation and high tunability, position our design at the forefront of dynamic nanoscale thermal management solutions. Looking ahead, future developments could involve integrating attosecond laser pulses and exploring suitable transient polariton modes to unlock even faster switching speeds and higher cooling efficiencies. This work underscores the strong potential of photodriven transient polaritons to revolutionize ultrafast thermal switching and lays the groundwork for significant advancements in ultrafast cooling technologies.

METHODS

Near-Field Radiative Heat Transfer. In our model, we consider pulsed laser excitation of WSe_2 with photon energies below its

bandgap. This excitation directly generates excitons without significantly altering the electron and hole distributions in the conduction and valence bands. These excitons then decay with a characteristic time constant τ, typically on the order of tens of picoseconds (ps), as discussed below. Given that the laser pulse duration is much shorter (~fs) than τ, we assume an instantaneous rise in the exciton population at $\Delta t = 0$. Additionally, since τ is significantly longer than the optical periods associated with the radiative transitions mediating heat transfer, we treat these transitions in a quasi-stationary regime. This assumption allows us to consider the exciton population as relatively constant over several optical cycles.

Under these conditions, we describe RHT flux in a quasi-stationary manner at each time point within the exciton decay time. To quantify near-field RHT Q (the power per unit area) across a vacuum gap of size d between two planar surfaces, we employ the framework of fluctuational electrodynamics, as described by[49]

$$Q(T_h, T_c, d) = \frac{1}{4\pi^2}\int_0^\infty d\omega[\Theta(\omega, T_h) - \Theta(\omega, T_c)] \int_0^\infty k_{\|}dk_{\|}[\xi_s(\omega, k_{\|}) + \xi_p(\omega, k_{\|})] \quad (6)$$

where $\Theta(\omega, T) = \hbar\omega/[\exp(\hbar\omega/k_BT) - 1]$ is the mean energy of a Planck oscillator, ω is the angular frequency, $k_{\|}$ is the modulus of the in-plane wave vector, T_h and T_c are the temperatures of the two terminals (hot and cold, respectively, under dynamic equilibrium conditions), and ξ_s and ξ_p are the photon transmission probabilities (PTP) associated with s- and p-polarized [i.e., transverse electric (TE) and transverse magnetic (TM)] modes, denoting the respective spectral decomposition of RHC. More precisely,

$$\xi^{1,2}_{n=s,p}(\omega, k_{\|}) = \begin{cases} \dfrac{(1 - |R_n^1|^2)(1 - |R_n^2|^2)}{|D_j|^2}, & k_{\|} \le k_0 \\ \dfrac{4\mathrm{Im}\{R_n^1\}\mathrm{Im}\{R_n^2\}e^{-2|k_{z0}|d}}{|D_j|^2}, & k_{\|} > k_0 \end{cases} \quad (7)$$

where $D_j = 1 - R_n^1R_n^2e^{2ik_{z0}d}$ in the denominator captures the Fabry-Pérot multiple interactions between the two surfaces; the subscript n (= s or p) runs over s or p polarizations; the superscripts 1 and 2 denote the emitter and receiver, respectively; $k_0 = \omega/c$ is the light wave vector in vacuum; $k_{z0} = (k_0^2 - k_{\|}^2)^{1/2}$ is the out-of-plane wave vector; and R_n is the total Fresnel reflection coefficient of each terminal surface. Incidentally, in accordance with the assumed retarded response formalism, k_0 is supplemented with an infinitesimal imaginary part and the square root is taken to yield $\mathrm{Im}\{k_{z0}\} > 0$. In addition, for suspended thin films and in-plane wave vectors $k_{\|} \le k_0$ (i.e., within the light cone), the factors $1 - |R_n|^2$ in eq 7 should be replaced by $1 - |R_n|^2 - |T_n|^2$, where $T_n$is the Fresnel transmission coefficient.[42,50]

ASSOCIATED CONTENT

Supporting Information

The Supporting Information is available free of charge at https://pubs.acs.org/doi/10.1021/acsnano.4c14188.

Fresnel coefficients used in the present study; dielectric response of graphene; analytic calculation for energy absorption in a gap-separated WSe_2/graphene heterostructure; carrier dynamics in WSe_2; temperature dependence of the dielectric response of WSe_2; thermal switching based on monolayer WSe_2; dynamic polaritonic coupling for ultrafast thermal switching; high tunability of the ultrafast thermal switch; comparison of performance relative to existing thermal switches (PDF)

AUTHOR INFORMATION

Corresponding Authors

F. Javier García de Abajo − *ICFO-Institut de Ciencies Fotoniques, The Barcelona Institute of Science and Technology, Castelldefels, Barcelona 08860, Spain; ICREA-Institució Catalana de Recerca i Estudis Avançats, Barcelona 08010, Spain;* orcid.org/0000-0002-4970-4565; Email: javier.garciadeabajo@nanophotonics.es

Qing Dai − *School of Materials Science and Engineering, Shanghai Jiao Tong University, Shanghai 200240, China; CAS Key Laboratory of Nanophotonic Materials and Devices, CAS Key Laboratory of Standardization and Measurement for Nanotechnology, National Center for Nanoscience and Technology, Beijing 100190, China; Center of Materials Science and Optoelectronics Engineering, University of Chinese Academy of Sciences, Beijing 100049, China;* orcid.org/0000-0002-1750-0867; Email: daiqing@sjtu.edu.cn

Authors

Bei Yang − *School of Materials Science and Engineering, Shanghai Jiao Tong University, Shanghai 200240, China;* orcid.org/0000-0002-0976-0650

Bai Song − *College of Engineering, Peking University, Beijing 100871, China; National Key Laboratory of Advanced MicroNanoManufacture Technology, Beijing 100871, China;* orcid.org/0000-0003-3013-9831

Complete contact information is available at: https://pubs.acs.org/10.1021/acsnano.4c14188

Author Contributions

Q.D. and B.Y. conceived the idea. Q.D., F.J.G.A., and B.S. supervised the project. B.Y. developed the theory, performed the calculations, and prepared the figures. B.Y., Q.D., F.J.G.A., and B.S. analyzed the data and discussed the results. B.Y. and Q.D. cowrote the manuscript, with valuable input and comments from B.S. and F.J.G.A.

Notes

The authors declare no competing financial interest.

ACKNOWLEDGMENTS

The authors greatly acknowledge the financial support from the National Natural Science Foundation of China (nos. 52302230, 51925203, and 52076002), the National Key Research and Development Program of China (no. 2022YFE0129700), and the Strategic Priority Research Program of the Chinese Academy of Sciences (no. XDB36000000).

REFERENCES

(1) Wehmeyer, G.; Yabuki, T.; Monachon, C.; Wu, J.; Dames, C. Thermal Diodes, Regulators, and Switches: Physical Mechanisms and Potential Applications. *Appl. Phys. Rev.* **2017**, *4* (4), No. 041304.

(2) Klinar, K.; Kitanovski, A. Thermal Control Elements for Caloric Energy Conversion. *Renew. Sustain. Energy Rev.* **2020**, *118* (June 2019), No. 109571.

(3) Swoboda, T.; Klinar, K.; Yalamarthy, A. S.; Kitanovski, A.; Muñoz Rojo, M. Solid-State Thermal Control Devices. *Adv. Electron. Mater.* **2021**, *7* (3), No. 2000625.

(4) McCaughan, A. N.; Verma, V. B.; Buckley, S. M.; Allmaras, J. P.; Kozorezov, A. G.; Tait, A. N.; Nam, S. W.; Shainline, J. M. A Superconducting Thermal Switch with Ultrahigh Impedance for

Interfacing Superconductors to Semiconductors. *Nat. Electron.* **2019**, *2* (10), 451−456.
(5) Ben-Abdallah, P.; Biehs, S. A. Near-Field Thermal Transistor. *Phys. Rev. Lett.* **2014**, *112* (4), 1−5.
(6) Mandrusiak, G.; She, X.; Waddell, A. M.; Acharya, S. On the Transient Thermal Characteristics of Silicon Carbide Power Electronics Modules. *IEEE Trans. Power Electron.* **2018**, *33* (11), 9783−9789.
(7) Corbett, S.; Gautam, D.; Lal, S.; Yu, K.; Balla, N.; Cunningham, G.; Razeeb, K. M.; Enright, R.; McCloskey, D. Electrodeposited Thin-Film Micro-Thermoelectric Coolers with Extreme Heat Flux Handling and Microsecond Time Response. *ACS Appl. Mater. Interfaces* **2021**, *13* (1), 1773−1782.
(8) Du, T.; Xiong, Z.; Delgado, L.; Liao, W.; Peoples, J.; Kantharaj, R.; Chowdhury, P. R.; Marconnet, A.; Ruan, X. Wide Range Continuously Tunable and Fast Thermal Switching Based on Compressible Graphene Composite Foams. *Nat. Commun.* **2021**, *12* (1), 4915.
(9) Hu, P.; Wang, J.; Zhang, P.; Wu, F.; Cheng, Y.; Wang, J.; Sun, Z. Hyperelastic Kevlar Nanofiber Aerogels as Robust Thermal Switches for Smart Thermal Management. *Adv. Mater.* **2023**, *35* (3), 1−12.
(10) Adams, M. J.; Verosky, M.; Zebarjadi, M.; Heremans, J. P. High Switching Ratio Variable-Temperature Solid-State Thermal Switch Based on Thermoelectric Effects. *Int. J. Heat Mass Transfer* **2019**, *134*, 114−118.
(11) Wang, Y.; Ren, J. Strain-Driven Switchable Thermal Conductivity in Ferroelastic PdSe2. *ACS Appl. Mater. Interfaces* **2021**, *13* (29), 34724−34731.
(12) Wu, C.; Zhao, Y.; Zhang, G.; Liu, C. Electronic. *Nanoscale Horizons* **2023**, *8* (2), 202−210.
(13) Cazorla, C.; Rurali, R. Dynamical Tuning of the Thermal Conductivity via Magnetophononic Effects. *Phys. Rev. B* **2022**, *105* (10), No. 104401.
(14) Qin, G.; Wang, H.; Zhang, L.; Qin, Z.; Hu, M. Giant Effect of Spin−Lattice Coupling on the Thermal Transport in Two-Dimensional Ferromagnetic CrI3. *J. Mater. Chem. C* **2020**, *8* (10), 3520−3526.
(15) Kommandur, S.; Kishore, R. A. Contact-Based Passive Thermal Switch with a High Rectification Ratio. *ACS Eng. Au* **2023**, *3* (2), 76−83.
(16) Tso, C. Y.; Chao, C. Y. H. Solid-State Thermal Diode with Shape Memory Alloys. *Int. J. Heat Mass Transfer* **2016**, *93*, 605−611.
(17) Chen, M. E.; Rojo, M. M.; Lian, F.; Koeln, J.; Sood, A.; Bohaichuk, S. M.; Neumann, C. M.; Garrow, S. G.; Goodson, K. E.; Alleyne, A. G.; Pop, E. Graphene-Based Electromechanical Thermal Switches. *2D Mater.* **2021**, *8* (3), No. 035055.
(18) Li, M.; Wu, H.; Avery, E. M.; Qin, Z.; Goronzy, D. P.; Nguyen, H. D.; Liu, T.; Weiss, P. S.; Hu, Y. Electrically Gated Molecular Thermal Switch. *Science (80-.).* **2023**, *382* (6670), 585−589.
(19) Liu, C.; Si, Y.; Zhang, H.; Wu, C.; Deng, S.; Dong, Y.; Li, Y.; Zhuo, M.; Fan, N.; Xu, B.; Lu, P.; Zhang, L.; Lin, X.; Liu, X.; Yang, J.; Luo, Z.; Das, S.; Bellaiche, L.; Chen, Y.; Chen, Z. Low Voltage-Riven High-Performance Thermal Switching in Antiferroelectric PbZrO3 Thin Films. *Science* **2023**, *382* (December), 1265−1269.
(20) Crossno, J.; Shi, J. K.; Wang, K.; Liu, X.; Harzheim, A.; Lucas, A.; Sachdev, S.; Kim, P.; Taniguchi, T.; Watanabe, K.; Ohki, T. A.; Fong, K. C. Observation of the Dirac Fluid and the Breakdown of the Wiedemann-Franz Law in Graphene. *Science (80-.).* **2016**, *351* (6277), 1058−1061.
(21) Ito, K.; Nishikawa, K.; Miura, A.; Toshiyoshi, H.; Iizuka, H. Dynamic Modulation of Radiative Heat Transfer beyond the Blackbody Limit. *Nano Lett.* **2017**, *17* (7), 4347−4353.
(22) Ilic, O.; Thomas, N. H.; Christensen, T.; Sherrott, M. C.; Soljačić, M.; Minnich, A. J.; Miller, O. D.; Atwater, H. A. Active Radiative Thermal Switching with Graphene Plasmon Resonators. *ACS Nano* **2018**, *12* (3), 2474−2481.
(23) Thomas, N. H.; Sherrott, M. C.; Broulliet, J.; Atwater, H. A.; Minnich, A. J. Electronic Modulation of Near-Field Radiative Transfer in Graphene Field Effect Heterostructures. *Nano Lett.* **2019**, *19* (6), 3898−3904.
(24) Shi, K.; Chen, Z.; Xing, Y.; Yang, J.; Xu, X.; Evans, J. S.; He, S. Near-Field Radiative Heat Transfer Modulation with an Ultrahigh Dynamic Range through Mode Mismatching. *Nano Lett.* **2022**, *22* (19), 7753−7760.
(25) Thompson, D.; Zhu, L.; Meyhofer, E.; Reddy, P. Nanoscale Radiative Thermal Switching via Multi-Body Effects. *Nat. Nanotechnol.* **2020**, *15* (2), 99−104.
(26) Yu, R.; Manjavacas, A.; García de Abajo, F. J. Ultrafast Radiative Heat Transfer. *Nat. Commun.* **2017**, *8* (1), 2.
(27) Huber, M. A.; Mooshammer, F.; Plankl, M.; Viti, L.; Sandner, F.; Kastner, L. Z.; Frank, T.; Fabian, J.; Vitiello, M. S.; Cocker, T. L.; Huber, R. Femtosecond Photo-Switching of Interface Polaritons in Black Phosphorus Heterostructures. *Nat. Nanotechnol.* **2017**, *12* (3), 207−211.
(28) Ni, G. X.; Wang, L.; Goldflam, M. D.; Wagner, M.; Fei, Z.; McLeod, A. S.; Liu, M. K.; Keilmann, F.; Özyilmaz, B.; Castro Neto, A. H.; Hone, J.; Fogler, M. M.; Basov, D. N. Ultrafast Optical Switching of Infrared Plasmon Polaritons in High-Mobility Graphene. *Nat. Photonics* **2016**, *10* (4), 244−247.
(29) Basov, D. N.; Fogler, M. M. Quantum Materials: The Quest for Ultrafast Plasmonics. *Nat. Nanotechnol.* **2017**, *12* (3), 187−188.
(30) Hu, D.; Chen, K.; Chen, X.; Guo, X.; Liu, M.; Dai, Q. Tunable Modal Birefringence in a Low-Loss Van Der Waals Waveguide. *Adv. Mater.* **2019**, *31* (27), 1−7.
(31) Mak, K. F.; Shan, J. Photonics and Optoelectronics of 2D Semiconductor Transition Metal Dichalcogenides. *Nat. Photonics* **2016**, *10* (4), 216−226.
(32) Wang, G.; Chernikov, A.; Glazov, M. M.; Heinz, T. F.; Marie, X.; Amand, T.; Urbaszek, B. Colloquium: Excitons in Atomically Thin Transition Metal Dichalcogenides. *Rev. Mod. Phys.* **2018**, *90* (2), 21001.
(33) Hu, D.; Yang, X.; Li, C.; Liu, R.; Yao, Z.; Hu, H.; Corder, S. N. G.; Chen, J.; Sun, Z.; Liu, M.; Dai, Q. Probing Optical Anisotropy of Nanometer-Thin van Der Waals Microcrystals by near-Field Imaging. *Nat. Commun.* **2017**, *8* (1), 1471.
(34) Arora, A.; Koperski, M.; Nogajewski, K.; Marcus, J.; Faugeras, C.; Potemski, M. Excitonic Resonances in Thin Films of WSe2: From Monolayer to Bulk Material. *Nanoscale* **2015**, *7* (23), 10421−10429.
(35) Liu, H.-L.; Yang, T.; Chen, J.-H.; Chen, H.-W.; Guo, H.; Saito, R.; Li, M.-Y.; Li, L.-J. Temperature-Dependent Optical Constants of Monolayer MoS2, MoSe2, WS2, and WSe2: Spectroscopic Ellipsometry and First-Principles Calculations. *Sci. Rep.* **2020**, *10* (1), 15282.
(36) Poellmann, C.; Steinleitner, P.; Leierseder, U.; Nagler, P.; Plechinger, G.; Porer, M.; Bratschitsch, R.; Schüller, C.; Korn, T.; Huber, R. Resonant Internal Quantum Transitions and Femtosecond Radiative Decay of Excitons in Monolayer WSe2. *Nat. Mater.* **2015**, *14* (9), 889−893.
(37) Steinleitner, P.; Merkl, P.; Nagler, P.; Mornhinweg, J.; Schüller, C.; Korn, T.; Chernikov, A.; Huber, R. Direct Observation of Ultrafast Exciton Formation in a Monolayer of WSe2. *Nano Lett.* **2017**, *17* (3), 1455−1460.
(38) Sternbach, A. J.; Chae, S. H.; Latini, S.; Rikhter, A. A.; Shao, Y.; Li, B.; Rhodes, D.; Kim, B.; Schuck, P. J.; Xu, X.; Zhu, X.-Y.; Averitt, R. D.; Hone, J.; Fogler, M. M.; Rubio, A.; Basov, D. N. Programmable Hyperbolic Polaritons in van Der Waals Semiconductors. *Science (80-.).* **2021**, *371* (6529), 617−620.
(39) Siday, T.; Sandner, F.; Brem, S.; Zizlsperger, M.; Perea-Causin, R.; Schiegl, F.; Nerreter, S.; Plankl, M.; Merkl, P.; Mooshammer, F.; Huber, M. A.; Malic, E.; Huber, R. Ultrafast Nanoscopy of High-Density Exciton Phases in WSe2. *Nano Lett.* **2022**, *22* (6), 2561−2568.
(40) Deng, S.; Chen, H. Ultrafast Generation of Optical Hyperbolicity. *Science (80-.).* **2021**, *371* (6529), 572−573.
(41) Yang, B.; Dai, Q. Highly-Efficient Radiative Thermal Rectifiers Based on near-Field Gap Variations. *Nanoscale* **2022**, *14* (45), 16978−16985.

(42) Yang, B.; Pan, D.; Guo, X.; Hu, H.; Dai, Q. Substrate Effects on the Near-Field Radiative Heat Transfer between Bi-Planar Graphene/HBN Heterostructures. *Int. J. Therm. Sci.* **2022**, *176* (January), No. 107493.
(43) Jin, C.; Kim, J.; Wu, K.; Chen, B.; Barnard, E. S.; Suh, J.; Shi, Z.; Drapcho, S. G.; Wu, J.; Schuck, P. J.; Tongay, S.; Wang, F. On Optical Dipole Moment and Radiative Recombination Lifetime of Excitons in WSe2. *Adv. Funct. Mater.* **2017**, *27* (19), 1−5.
(44) Basov, D. N.; Fogler, M. M.; García de Abajo, F. J. Polaritons in van Der Waals Materials. *Science (80-.).* **2016**, *354* (6309), aag1992.
(45) Guo, X.; Lyu, W.; Chen, T.; Luo, Y.; Wu, C.; Yang, B.; Sun, Z.; García de Abajo, F. J.; Yang, X.; Dai, Q. Polaritons in Van Der Waals Heterostructures. *Adv. Mater.* **2023**, *35* (17), No. 2201856.
(46) Fu, R.; Qu, Y.; Xue, M.; Liu, X.; Chen, S.; Zhao, Y.; Chen, R.; Li, B.; Weng, H.; Liu, Q.; Dai, Q.; Chen, J. Manipulating Hyperbolic Transient Plasmons in a Layered Semiconductor. *Nat. Commun.* **2024**, *15* (1), 1−8.
(47) del Águila, A. G.; Wong, Y. R.; Wadgaonkar, I.; Fieramosca, A.; Liu, X.; Vaklinova, K.; Dal Forno, S.; Do, T. T. H.; Wei, H. Y.; Watanabe, K.; Taniguchi, T.; Novoselov, K. S.; Koperski, M.; Battiato, M.; Xiong, Q. Ultrafast Exciton Fluid Flow in an Atomically Thin MoS2 Semiconductor. *Nat. Nanotechnol.* **2023**, *18* (9), 1012−1019.
(48) Inoue, T.; Morita, R.; Nigo, K.; Yoshida, M.; De Zoysa, M.; Ishizaki, K.; Noda, S. Self-Evolving Photonic Crystals for Ultrafast Photonics. *Nat. Commun.* **2023**, *14* (1), 1−7.
(49) Sergei, M. R.; Yurii, A. K.; Valeryan, I. T. *Principles of Statistical Radiophysics*; Springer:: New York, 1989.
(50) Li, Q.; He, H.; Chen, Q.; Song, B. Thin-Film Radiative Thermal Diode with Large Rectification. *Phys. Rev. Appl.* **2021**, *16* (1), No. 014069.